

# Spin-lattice coupling in frustrated antiferromagnets

Oleg Tchernyshyov<sup>1</sup> and Gia-Wei Chern<sup>2</sup>

<sup>1</sup> Department of Physics and Astronomy, Johns Hopkins University, 3400 N. Charles St., Baltimore, MD 21218, U. S. A.

<sup>2</sup> Department of Physics, University of Wisconsin, 1150 University Avenue, Madison, WI 53706, U. S. A.

We review the mechanism of spin-lattice coupling in relieving the geometrical frustration of pyrochlore antiferromagnets, in particular spinel oxides. The tetrahedral unit, which is the building block of the pyrochlore lattice, undergoes a spin-driven Jahn-Teller instability when lattice degrees of freedom are coupled to the antiferromagnetism. By restricting our considerations to distortions which preserve the translational symmetries of the lattice, we present a general theory of the collective spin-Jahn-Teller effect in the pyrochlore lattice. One of the predicted lattice distortions breaks the inversion symmetry and gives rise to a chiral pyrochlore lattice, in which frustrated bonds form helices with a definite handedness. The chirality is transferred to the spin system through spin-orbit coupling, resulting in a long-period spiral state, as observed in spinel  $\text{CdCr}_2\text{O}_4$ . We discuss explicit models of spin-lattice coupling using local phonon modes, and their applications in other frustrated magnets.

## 1.1 Introduction

As explained in the introductory chapter by Chalker, sufficiently strong frustration in a magnet results in a large degeneracy of its ground-state manifold. Prime examples of this behavior are Heisenberg antiferromagnets on the kagome [1, 2] and pyrochlore [3, 4] lattices with interactions restricted to nearest-neighbor sites. In the classical limit of a large spin  $S$ , the ground states of these magnets exhibit very high, continuous degeneracies and possess numerous zero modes, which correspond to moving the system through its manifold of ground states [5]. The pyrochlore antiferromagnet represents a particularly striking example of high ground-state degeneracy: at least half of its spin-wave modes have zero frequencies in any collinear ground state [4].

A large degeneracy means enhanced sensitivity to perturbations, even when these are nominally weak. In this chapter we will consider a coupling

between spins and the underlying lattice, which has its origin in the dependence of the exchange integrals on the atomic positions,  $J(\mathbf{r}_1, \mathbf{r}_2) \mathbf{S}_1 \cdot \mathbf{S}_2$ , and is known as magnetoelastic exchange [6]. In the pyrochlore antiferromagnet, this coupling lifts the degeneracy of the classical ground states and induces a symmetry-lowering distortion of the lattice, in analogy with the spin-Peierls effect in antiferromagnetic spin chains [7]. A spin-Peierls-like phase transition has been observed in several antiferromagnetic spinels where the magnetic ions form the pyrochlore lattice [8–10].

The problem of coupled spins and lattice degrees of freedom in a pyrochlore antiferromagnet is reminiscent of the collective Jahn-Teller effect [11] in crystalline solids. We therefore begin the discussion by studying the Jahn-Teller distortion in a tetrahedral “molecule” with four spins, which is the structural unit of the pyrochlore lattice. A symmetry-based analysis will be supplemented by models with specific spin-phonon coupling mechanisms. We will then extend the analysis to an infinite lattice, to examine some of the possible ground states of the classical spin system. In concluding this chapter, we will test the theory of spin-phonon coupling on the example of  $\text{CdCr}_2\text{O}_4$ , a frustrated Heisenberg antiferromagnet with  $S = 3/2$  spins residing on the pyrochlore lattice.

## 1.2 Spin-driven Jahn-Teller effect in a tetrahedron

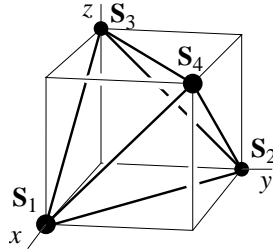


**Fig. 1.1.** Representation of four spins in the corners of a regular tetrahedron.

Consider the basic structural unit of the pyrochlore lattice, a cluster in the shape of a regular tetrahedron with four spins of length  $S$  at the corners (Fig. 1.1). The Heisenberg exchange energy depends on the total spin of the cluster,  $\mathbf{S}_{\text{tot}} = \sum_{i=1}^4 \mathbf{S}_i$ , according to

$$H_0 = J \sum_{i < j} \mathbf{S}_i \cdot \mathbf{S}_j = \frac{JS_{\text{tot}}^2}{2} - \text{const.} \quad (1.1)$$

For antiferromagnetic exchange ( $J > 0$ ), this energy is minimized when the total spin of the cluster is 0. The degeneracy of the ground state is thus equal to the number of distinct spin-singlet states in a system of four spins.

For spins of length  $S$ , the number of linearly independent singlet ground states is  $2S + 1$ . Indeed, the pair of spins 1 and 2 can have a total combined spin  $\mathbf{S}_{12}$  ranging from 0 to  $2S$ . The same is true of the spin pair 3 and 4. A state with a total spin  $S_{\text{tot}} = 0$  can be obtained by combining states with  $S_{12} = S_{34} = 0$ ,  $S_{12} = S_{34} = 1$ , and so on, up to  $S_{12} = S_{34} = 2S$ . Thus one observes that, for any spin length  $S$ , the ground state of the four spins is degenerate. The high symmetry of the cluster means that, in accordance with the Jahn-Teller theorem,<sup>3</sup> the ground-state energy can be lowered through a distortion.

Assume for simplicity (a more general case will be considered below) that the exchange coupling  $J$  between spins  $i$  and  $j$  has a dependence on their separation,  $r_{ij} = |\mathbf{r}_i - \mathbf{r}_j|$ , given by

$$J(r_{ij}) = J(\bar{r}_{ij}) + J'(\bar{r}_{ij})\delta r_{ij} + J''(\bar{r}_{ij})\delta r_{ij}^2/2 + \dots, \quad (1.2)$$

where  $\bar{r}_{ij}$  is a reference distance. At zeroth order in the displacements  $\delta \mathbf{r}_i$ , we recover the unperturbed Heisenberg Hamiltonian (1.1) with  $2S + 1$  degenerate singlet ground states.

The first-order term,

$$H_1 = J' \sum_{i < j} (\mathbf{S}_i \cdot \mathbf{S}_j) \delta r_{ij}, \quad (1.3)$$

lifts the degeneracy of the ground-state manifold. As long as the displacements involved remain small enough to satisfy  $J' \delta r_{ij} \ll J$ , excited states with  $S_{\text{tot}} > 0$  at energies  $J$  and higher may be neglected. Thus it is necessary to determine the energy levels of  $H_1$  in the Hilbert space of the singlet ground states.

### 1.2.1 Generalized coordinates and forces

The perturbation Hamiltonian (1.3) depends on the atomic displacements  $\delta \mathbf{r}_i$ , which comprise  $4 \times 3 = 12$  degrees of freedom. However, not all of these will influence the exchange energy of the spins. As one example, this does not change under rigid translations of the tetrahedron (3 modes) or under global rotations (a further 3 modes). The remaining 6 modes represent various deformations of the four-site cluster. To facilitate further analysis, we classify these modes in terms of the irreducible representations (irreps) of the tetrahedral point group  $T_d$  [13].

The 6 modes belong to three irreps of  $T_d$ . The breathing mode (irrep  $A$ ) leaves the symmetry of the tetrahedron fully intact. A doublet of tetragonal

---

<sup>3</sup>It is important to note that the degeneracy is not caused by the symmetry of time reversal, so the conditions of the theorem are fulfilled [12].

and orthorhombic distortions,  $\mathbf{Q}^E = (Q_1^E, Q_2^E)$ , transforms under irrep  $E$ . Finally, a triplet  $\mathbf{Q}^{T_2} = (Q_1^{T_2}, Q_2^{T_2}, Q_3^{T_2})$ , transforming as irrep  $T_2$ , elongates and compresses opposing bonds; equal-amplitude superpositions of the triplet components yield trigonal distortions. The coordinates of these modes can be expressed in terms of Cartesian displacements of the spins with the coefficients listed in Table 1.1.

**Table 1.1.** Coefficients relating the 6 distortions of a tetrahedron to the displacements  $\delta \mathbf{r}_i$  of its vertices. The reference frame is shown in Fig. 1.1.

		$\delta x_1$	$\delta y_1$	$\delta z_1$	$\delta x_2$	$\delta y_2$	$\delta z_2$	$\delta x_3$	$\delta y_3$	$\delta z_3$	$\delta x_4$	$\delta y_4$	$\delta z_4$
$A$	$Q^A$	$+\frac{1}{\sqrt{12}}$	$-\frac{1}{\sqrt{12}}$	$-\frac{1}{\sqrt{12}}$	$-\frac{1}{\sqrt{12}}$	$+\frac{1}{\sqrt{12}}$	$-\frac{1}{\sqrt{12}}$	$-\frac{1}{\sqrt{12}}$	$-\frac{1}{\sqrt{12}}$	$+\frac{1}{\sqrt{12}}$	$+\frac{1}{\sqrt{12}}$	$+\frac{1}{\sqrt{12}}$	$+\frac{1}{\sqrt{12}}$
$E$	$Q_1^E$	$-\frac{1}{\sqrt{24}}$	$+\frac{1}{\sqrt{24}}$	$-\frac{1}{\sqrt{6}}$	$+\frac{1}{\sqrt{24}}$	$-\frac{1}{\sqrt{24}}$	$-\frac{1}{\sqrt{6}}$	$+\frac{1}{\sqrt{24}}$	$+\frac{1}{\sqrt{24}}$	$+\frac{1}{\sqrt{6}}$	$-\frac{1}{\sqrt{24}}$	$-\frac{1}{\sqrt{24}}$	$+\frac{1}{\sqrt{6}}$
	$Q_2^E$	$+\frac{1}{\sqrt{8}}$	$+\frac{1}{\sqrt{8}}$	0	$-\frac{1}{\sqrt{8}}$	$-\frac{1}{\sqrt{8}}$	0	$-\frac{1}{\sqrt{8}}$	$+\frac{1}{\sqrt{8}}$	0	$+\frac{1}{\sqrt{8}}$	$-\frac{1}{\sqrt{8}}$	0
$T_2$	$Q_1^{T_2}$	0	$+\frac{1}{\sqrt{8}}$	$+\frac{1}{\sqrt{8}}$	0	$+\frac{1}{\sqrt{8}}$	$-\frac{1}{\sqrt{8}}$	0	$-\frac{1}{\sqrt{8}}$	$+\frac{1}{\sqrt{8}}$	0	$-\frac{1}{\sqrt{8}}$	$-\frac{1}{\sqrt{8}}$
	$Q_2^{T_2}$	$+\frac{1}{\sqrt{8}}$	0	$-\frac{1}{\sqrt{8}}$	$+\frac{1}{\sqrt{8}}$	0	$+\frac{1}{\sqrt{8}}$	$-\frac{1}{\sqrt{8}}$	0	$+\frac{1}{\sqrt{8}}$	$-\frac{1}{\sqrt{8}}$	0	$-\frac{1}{\sqrt{8}}$
	$Q_3^{T_2}$	$+\frac{1}{\sqrt{8}}$	$-\frac{1}{\sqrt{8}}$	0	$-\frac{1}{\sqrt{8}}$	$+\frac{1}{\sqrt{8}}$	0	$+\frac{1}{\sqrt{8}}$	$+\frac{1}{\sqrt{8}}$	0	$-\frac{1}{\sqrt{8}}$	$-\frac{1}{\sqrt{8}}$	0

**Table 1.2.** Coefficients relating the bond elongations  $\delta r_{ij}$  to the distortion coordinates  $Q^A$ ,  $\mathbf{Q}^E = (Q_1^E, Q_2^E)$ , and  $\mathbf{Q}^{T_2} = (Q_1^{T_2}, Q_2^{T_2}, Q_3^{T_2})$ .

	$Q^A$	$Q_1^E$	$Q_2^E$	$Q_1^{T_2}$	$Q_2^{T_2}$	$Q_3^{T_2}$
$\delta r_{14}$	$+\sqrt{\frac{2}{3}}$	$+\frac{1}{\sqrt{12}}$	$-\frac{1}{2}$	-1	0	0
$\delta r_{23}$	$+\sqrt{\frac{2}{3}}$	$+\frac{1}{\sqrt{12}}$	$-\frac{1}{2}$	+1	0	0
$\delta r_{24}$	$+\sqrt{\frac{2}{3}}$	$+\frac{1}{\sqrt{12}}$	$+\frac{1}{2}$	0	-1	0
$\delta r_{13}$	$+\sqrt{\frac{2}{3}}$	$+\frac{1}{\sqrt{12}}$	$+\frac{1}{2}$	0	+1	0
$\delta r_{34}$	$+\sqrt{\frac{2}{3}}$	$-\frac{1}{\sqrt{3}}$	0	0	0	-1
$\delta r_{12}$	$+\sqrt{\frac{2}{3}}$	$-\frac{1}{\sqrt{3}}$	0	0	0	+1

By expressing the changes in bond lengths,  $\delta r_{ij}$ , in terms of the generalized coordinates, we reduce the perturbation Hamiltonian (1.3) to the form

$$H_1 = \sum_{\alpha} J^{\alpha'} \sum_n Q_n^{\alpha} f_n^{\alpha}, \quad (1.4)$$

where the index  $\alpha$  enumerates the irreps and  $n$  its components. The variable  $f_n^{\alpha}$  is the generalized force which is conjugate to the coordinate  $Q_n^{\alpha}$  and has the same symmetry properties.  $J^{\alpha'}$  is a coupling constant appropriate for the irrep  $\alpha$ .

For illustration, the breathing mode  $Q_A$  couples to the spin operator

$$f^A = \frac{1}{\sqrt{6}} \sum_{i < j} \mathbf{S}_i \cdot \mathbf{S}_j, \quad (1.5)$$

which is invariant under all symmetry operations of  $T_d$ . Further, up to a trivial factor, this is the unperturbed Hamiltonian (1.1) and so has the same value in any of the degenerate ground states. Consequently, the term  $-J^{A'} Q^A f^A$  in the perturbation Hamiltonian (1.3) produces a trivial energy shift of the degenerate ground states, but does not split them.

The triplet mode and the associated triplet force also do not induce a splitting. To demonstrate this, we note that  $Q_1^{T_2}$  couples to the operator

$$f_1^{T_2} = (\mathbf{S}_2 \cdot \mathbf{S}_3 - \mathbf{S}_1 \cdot \mathbf{S}_4)/\sqrt{2}, \quad (1.6)$$

which vanishes in any singlet state.<sup>4</sup> In the presence of an applied magnetic field, the triplet forces cannot be neglected because of the nonzero total spin  $S_{\text{tot}}$ . The triplet forces and the corresponding trigonal distortions play an important role in the stabilization of the half-magnetization plateaus observed in some spinel chromites (Sec. 1.3.1).

The only two modes involved in the splitting of the ground state are the components of the doublet  $(Q_1^E, Q_2^E)$  of tetragonal and orthorhombic distortions. These couple, respectively, to the spin operators

$$\begin{aligned} f_1^E &= \frac{\mathbf{S}_1 \cdot \mathbf{S}_4 + \mathbf{S}_2 \cdot \mathbf{S}_3 + \mathbf{S}_2 \cdot \mathbf{S}_4 + \mathbf{S}_1 \cdot \mathbf{S}_3 - 2\mathbf{S}_1 \cdot \mathbf{S}_2 - 2\mathbf{S}_3 \cdot \mathbf{S}_4}{\sqrt{12}}, \\ f_2^E &= \frac{\mathbf{S}_2 \cdot \mathbf{S}_4 + \mathbf{S}_1 \cdot \mathbf{S}_3 - \mathbf{S}_1 \cdot \mathbf{S}_4 - \mathbf{S}_2 \cdot \mathbf{S}_3}{2}. \end{aligned} \quad (1.7)$$

In what follows, we omit the irrep superscript because only the doublet  $E$  participates in lifting the degeneracy of the ground-state manifold.

In addition to the magnetoelastic exchange (1.3), which is linear in the distortion amplitude, it is necessary to consider also the elastic energy of the deformation. We thus obtain the spin-distortion Hamiltonian

$$H = J'(\mathbf{Q} \cdot \mathbf{f}) + k|\mathbf{Q}|^2/2 \equiv J'(Q_1 f_1 + Q_2 f_2) + k(Q_1^2 + Q_2^2)/2, \quad (1.8)$$

where  $k$  is the elastic constant of the doublet distortion. Having established this, the next task is to minimize the energy (1.8) with respect to both the coordinates and the spins.

### 1.2.2 Four $S = 1/2$ spins on a tetrahedron

The problem of four  $S = 1/2$  spins on a deformable tetrahedron was first analyzed by Yamashita and Ueda [14]. The ground state of the unperturbed

---

<sup>4</sup>Indeed, from  $\mathbf{S}_1 + \mathbf{S}_2 + \mathbf{S}_3 + \mathbf{S}_4 = 0$  it follows that  $(\mathbf{S}_1 + \mathbf{S}_4)^2 = (\mathbf{S}_2 + \mathbf{S}_3)^2$  and thus  $\mathbf{S}_1 \cdot \mathbf{S}_4 = \mathbf{S}_2 \cdot \mathbf{S}_3$ .

exchange Hamiltonian (1.1) is two-fold degenerate. As a basis in this Hilbert space one may use singlet states with a well-defined total spin on bonds 12 and 34,  $S_{12} = S_{34} = \sigma$ , where  $\sigma = 0$  or 1 [15]. In this basis, the force operators  $f_1$  and  $f_2$  are proportional to the Pauli matrices  $\sigma_1$  and  $\sigma_3$ , respectively, so that the Hamiltonian (1.8) reduces to

$$H = J'(Q_1\sigma_1 + Q_2\sigma_3)\sqrt{3}/2 + k(Q_1^2 + Q_2^2)/2. \quad (1.9)$$

For a given distortion  $\mathbf{Q}$ , the ground-state manifold is split into the two energy levels

$$E_{1,2} = \pm |J'|Q\sqrt{3}/2 + kQ^2/2, \quad (1.10)$$

and the energy of the system is minimized when  $Q = |J'|\sqrt{3}/(2k)$ . Note that this quantity depends on the magnitude of the distortion,  $Q = \sqrt{Q_1^2 + Q_2^2}$ , but not on its “direction:” it can be tetragonal, purely orthorhombic, or any combination of these. This degeneracy is associated with a continuous symmetry of the Hamiltonian (1.9) that involves simultaneous “rotations” of both the distortion coordinates and the Pauli matrices,

$$\begin{pmatrix} Q_1 \\ Q_2 \end{pmatrix} \mapsto \begin{pmatrix} \cos \theta & \sin \theta \\ -\sin \theta & \cos \theta \end{pmatrix} \begin{pmatrix} Q_1 \\ Q_2 \end{pmatrix}, \quad \begin{pmatrix} \sigma_1 \\ \sigma_3 \end{pmatrix} \mapsto \begin{pmatrix} \cos \theta & \sin \theta \\ -\sin \theta & \cos \theta \end{pmatrix} \begin{pmatrix} \sigma_1 \\ \sigma_3 \end{pmatrix}. \quad (1.11)$$

The invariance of the energy under this transformation does not reflect an underlying symmetry, and applies at the level of approximation used here. Terms of higher order in  $\mathbf{Q}$  break this symmetry to leave only a three-fold degeneracy, as may be expected on symmetry grounds [14]. The lowest-order anharmonic term allowed by the symmetry is proportional to

$$Q_x Q_y Q_z \equiv \left( -\frac{1}{2}Q_1 + \frac{\sqrt{3}}{2}Q_2 \right) \left( -\frac{1}{2}Q_1 - \frac{\sqrt{3}}{2}Q_2 \right) Q_1 = \frac{1}{4}Q^3 \cos 3\alpha, \quad (1.12)$$

where  $Q_x$ ,  $Q_y$ , and  $Q_z$  measure tetragonal distortions along the respective axes and  $\alpha$  is the polar angle in the  $(Q_1, Q_2)$  plane. Depending on the sign of the cubic term, it favors three distinct ground states at  $\alpha = 0, \pm 2\pi/3$  or at  $\alpha = \pi, \pm \pi/3$ . The former “vacua” have spin singlets on two opposing bonds (*e.g.*  $S_{12} = S_{34} = 0$  for  $\alpha = 0$ ) while the latter have spin triplets on two opposing bonds ( $S_{12} = S_{34} = 1$  for  $\alpha = \pi$ ). These ground states exhibit valence-bond order, which violates the point-group symmetry of the cluster but not the  $\text{SO}(3)$  symmetry of the exchange interaction. The two-component order parameter (1.7), introduced by Harris, Berlinsky and Bruder [16], measures the differences in spin correlations on the different bonds.

The ground states of the cluster exhibit a tetragonal lattice distortion along one of the three major axes with  $\mathbf{Q} = -J'\langle \mathbf{f} \rangle \sqrt{3}/(2k)$ . If  $J' < 0$ , as would be expected for direct antiferromagnetic exchange, the tetrahedron is flattened (elongated) in a ground state with triplets (singlets) on opposing bonds.

For spins of length  $S > 1/2$ , the analysis proceeds by a similar route [15]. The lowest-order perturbation (1.3) yields three degenerate singlet ground states with the largest possible spins on two opposing bonds, such as  $S_{12} = S_{34} = 2S$ , and a tetragonal distortion (a flattening of the tetrahedron for  $J' < 0$ ). This result is most easily understood in the classical limit  $S \rightarrow \infty$ , to which we turn next.

### 1.2.3 Four classical spins on a tetrahedron

For classical spins, the total energy  $E(\mathbf{f}, \mathbf{Q})$  (1.8) can be minimized in two steps. We minimize it first with respect to the distortion  $\mathbf{Q}$  at a fixed  $\mathbf{f}$ .<sup>5</sup> A minimum is achieved when  $\mathbf{Q} = -J'\mathbf{f}/k$ , yielding the energy

$$E(\mathbf{f}) = -J'^2 f^2 / (2k), \quad (1.13)$$

whence the total energy is minimized by states with the largest magnitude of the force doublet  $\mathbf{f}$ . Thus it is necessary to quantify the magnetoelastic forces in those states of the ground-state manifold with  $S_{\text{tot}} = 0$ .

The domain of attainable  $\mathbf{f}$  values forms a regular triangle in the  $(f_1, f_2)$  plane (Fig. 1.2). Its three corners correspond to the three distinct collinear states with four satisfied bonds ( $\mathbf{S}_i \cdot \mathbf{S}_j = -S^2$ ) and two frustrated ones ( $\mathbf{S}_i \cdot \mathbf{S}_j = +S^2$ ). States elsewhere on the perimeter of the triangle have coplanar spins.

Not unexpectedly, the doublet force is maximized (and the total energy minimized) in the collinear states. Indeed, in such states antiparallel spins attract and parallel spins repel each other with forces  $F = -J' \mathbf{S}_i \cdot \mathbf{S}_j$  of the largest possible magnitude,  $|J'|S^2$ . The large forces result in large distortions, yielding a large decrease in the total energy. Thus in the classical limit one expects collinear ground states in which the tetrahedron is flattened along one of the principal axes for  $J' < 0$ .<sup>6</sup>

### 1.2.4 Color notation and other useful analogies

We find it convenient here to introduce an analogy with the color triangle, where the vertices correspond to the primary colors red, green, and blue, the midpoints of the edges to the secondary colors cyan, magenta, and yellow, and the center to the absence of color. If we color bonds perpendicular to the major axes  $a$ ,  $b$ , and  $c$  respectively red, green, and blue, then the color of the state in Fig. 1.2 reflects the color of the frustrated bonds.

The collinear ground states obtained for classical spins provide a simple rationalization for the valence-bond states found for quantum spins of length

---

<sup>5</sup>This method cannot be applied to quantum spins because the operators  $f_1$  and  $f_2$  do not commute [15], and so their values cannot be measured simultaneously.

<sup>6</sup>If  $J' > 0$ , the spins are still collinear but the tetrahedron is elongated along the same axis.

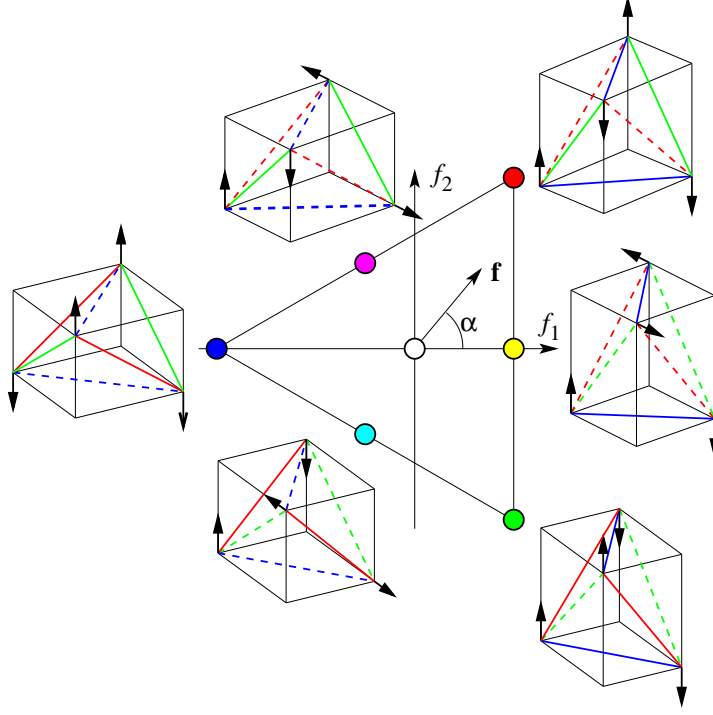


**Fig. 1.2.** The domain of attainable values of the force doublet  $\mathbf{f} = (f_1, f_2)$  (1.7) for classical spins. Dashed lines indicate frustrated bonds ( $\mathbf{S}_i \cdot \mathbf{S}_j \geq 0$ ). Reprinted with permission from Ref. [15].

$S > 1/2$  [15]. Quantum states maximizing the spins of opposing pairs (for example  $S_{12} = S_{34} = 2S$ ) are the analogs of the collinear classical configurations ( $S_1 = S_2 = -S_3 = -S_4$ ).

Lastly, we recall that the spin-distortion Hamiltonian (1.8) was derived for a simplified model of exchange in which the Heisenberg interaction strength  $J$  depends only on the separation of the two spins. This approximation is good for direct spin exchange [17], which is the dominant exchange interaction in the chromium spinels  $\text{ZnCr}_2\text{O}_4$  [18] and  $\text{CdCr}_2\text{O}_4$  [19], as well as in some other chromium antiferromagnets [20]. However, in other situations  $J$  may exhibit a more complex dependence on atomic displacements, such as the very sensitive bond-angle-dependence of superexchange. Fortunately, the form of the spin-distortion coupling derived above (1.8) is robust, as can be seen by symmetry considerations: group theory guarantees that there are no other invariant terms of the same order in  $\mathbf{f}$  and  $\mathbf{Q}$ . In the general case,  $J'$  represents a linear combination of exchange derivatives.



### 1.2.5 Spin-Jahn-Teller effect on a triangle

Another well-known lattice producing strong frustration in an antiferromagnet is the kagome geometry [1, 2], a network of corner-sharing triangles in a plane, and its three-dimensional variant, the hyperkagome lattice [21]. It is natural to ask whether spin-lattice coupling is also an effective mechanism for relieving frustration in this case. We answer this question by considering the building block of the kagome lattice, a triangle with three spins.

Classical Heisenberg spins interacting through antiferromagnetic Heisenberg exchange minimize their energy by making angles of  $120^\circ$  with one another. An analysis along the lines of Sec. 1.2 shows that the correction to the exchange energy from the magnetoelastic term is quadratic in the spin displacements: the linear term cancels. Without this linear term, a spontaneous distortion does not occur. The absence of the linear term can be understood simply from the magnetoelastic forces between the spins: the three forces, being proportional to the scalar products of the spins, are equal in a state where the spins make equal angles with each other. These symmetrical forces only shrink the triangle without distorting it.

The argument against the Jahn-Teller distortion fails if the quadratic term in the magnetoelastic correction is negative and large enough to overcome the purely elastic cost of the distortion, a scenario proposed recently by Wang and Vishwanath [22]. In our view, however, empirical evidence indicates that a Jahn-Teller instability of this sort would be a rare exception. The strength of the quadratic magnetoelastic term can be estimated from the splitting of degenerate phonons in antiferromagnets with a spin-induced Jahn-Teller distortion [18]. Such splittings, observed in  $\text{ZnCr}_2\text{O}_4$  [18],  $\text{CdCr}_2\text{O}_4$  [19], and  $\text{MnO}$  [23], do not exceed 12% of the phonon frequencies, which indicates the dominance of the purely elastic contribution.

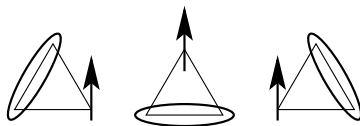


**Fig. 1.3.** Valence-bond ground states of three spins  $S = 1/2$  with antiferromagnetic Heisenberg exchange interactions. The ellipses designate singlet bonds.

While the spin-Jahn-Teller distortion of a triangle appears unlikely in the classical limit, the opposite extreme — quantum spins of length  $S = 1/2$  — are a completely different situation. The ground state of three such spins interacting through antiferromagnetic Heisenberg exchange is any state with a total spin  $S_\Delta = 1/2$ . Such a state is fourfold degenerate: part of this degeneracy is of the Kramers type, as the projection of the total spin on an arbitrary axis can be  $S_\Delta^z = \pm 1/2$ , and there is an additional twofold degeneracy related

to the symmetry of the triangle. This degeneracy can be understood in terms of valence-bond states, in which two of the spins on the triangle form a singlet bond (a quantum dimer) while the third remains free. Figure 1.3 shows three such states, although they are not mutually orthogonal; in fact only two of these states are linearly independent.

The presence of a non-Kramers degeneracy leads to the spin-Jahn-Teller effect on a triangle with spins  $S = 1/2$ . The analysis is similar to that for four  $S = 1/2$  spins on a tetrahedron (Sec. 1.2.2), with three distinct ground states. Depending on the sign of the cubic term, the distorted triangle will have either two long bonds and one short bond with a singlet on it, or two short bonds and one long bond with a triplet.

### 1.3 Models with local phonon modes

The symmetry-based analysis of the previous section is basically exact regardless of the underlying microscopic model for the phonons. In this section we review some specific models of spin-lattice coupling based on local phonon modes and also discuss their applications.

Probably the simplest situation is the “bond-phonon model,” in which the exchange integral (1.3) and also the elastic energy depend only on the bond length  $r_{ij}$ . The elastic energy is approximated by the sum of individual terms  $k\delta r_{ij}^2/2$ . After integrating out the bond variables  $\delta r_{ij}$ , the model generates a biquadratic spin Hamiltonian

$$-(J'^2/2k) \sum_{\langle ij \rangle} (\mathbf{S}_i \cdot \mathbf{S}_j)^2, \quad (1.14)$$

which clearly favors collinear spin configurations. Because of its simplicity, this model has been applied in numerous studies of frustrated magnets. As one example, Becca *et al.* found using the bond-phonon model that magnetoelastic coupling leads to a spin-Peierls transition in the frustrated  $J_1$ - $J_2$  antiferromagnet on the square lattice [24, 25]. This study may be relevant to the nature of the transition to a phase of collinear order observed in the quasi-2D antiferromagnet  $\text{Li}_2\text{VOSiO}_4$ .

On the pyrochlore lattice, the bond-phonon model gives a ground state with  $3^N$ -fold degeneracy, where  $N$  is the total number of tetrahedra: each tetrahedron can be flattened along one of the 3 major axes, independently of the other tetrahedra. A more realistic phonon model can be formulated in terms of the independent displacements of each atom, with the bond lengths determined from these atomic displacements by  $\delta r_{ij} = (\mathbf{u}_i - \mathbf{u}_j) \cdot \hat{\mathbf{r}}_{ij}$ . This is known as the site-phonon (or Einstein phonon) model of spin-lattice coupling [26, 27], in the simplest version of which the elastic energy is approximated by a sum of individual terms  $k|\mathbf{u}_i|^2/2$ , an assumption which leads to a constant dispersion similar to the long-wavelength limit of optical phonons. In addition

to Eq. (1.14), after integrating out the displacements the model introduces couplings between bond variables,

$$-(J^2/2k) \sum_{i,j \neq k} (\hat{\mathbf{r}}_{ij} \cdot \hat{\mathbf{r}}_{ik}) (\mathbf{S}_i \cdot \mathbf{S}_j) (\mathbf{S}_i \cdot \mathbf{S}_k). \quad (1.15)$$

Because of these coupling terms, coherent long-range distortions are possible in this model. Using the site-phonon model, Wang and Vishwanath [22] showed that a zigzag collinear order of the triangular antiferromagnet  $\text{CuFeO}_2$  is a ground state of the spin-lattice Hamiltonian. However, because the  $\text{Fe}^{3+}$  ion in this compound has spin  $S = 5/2$  and  $L = 0$ , resulting in a rather small magnetic anisotropy, a relatively large spin-lattice coupling is required to induce the zigzag collinear order from the non-collinear  $120^\circ$  ground state of Heisenberg spins on this lattice.

In the context of the pyrochlore lattice, the interaction term of Eq. (1.15) corresponds to an antiferromagnetic coupling between the force doublets of nearest-neighbor tetrahedra,  $K \sum_{\langle \alpha \beta \rangle} \mathbf{f}_\alpha \cdot \mathbf{f}_\beta$ , where the coupling constant  $K > 0$ . As a result, neighboring tetrahedra tend to be flattened along different directions (*e.g.*  $\langle 100 \rangle$  and  $\langle 010 \rangle$ ). While this reduces the total number of ground states, it still leaves a very high accidental degeneracy which grows exponentially with  $N$ .

### 1.3.1 Half-magnetization plateau in $\text{ACr}_2\text{O}_4$ spinels

Local phonon models provide an explicit description with which one may study the spin-lattice stabilization of the half-magnetization plateau observed in some spinel chromites. The low-temperature magnetization curves of the spinels  $\text{CdCr}_2\text{O}_4$  and  $\text{HgCr}_2\text{O}_4$  exhibit a sharp transition into a wide plateau region where the magnetization is equal to half its saturation value [28, 29]. Each tetrahedron in the half-plateau state is in one of the four 3-up-1-down collinear spin configurations. While thermal and quantum fluctuations act in general to favor collinear spins, and indeed in some cases help to stabilize the magnetization plateaus in frustrated magnets, the observed half-magnetization plateau in spinels arises most likely due to a coupling between the spins and the lattice, a scenario also supported by the observation of a spontaneous structural distortion accompanying the half-plateau transition.

Because the total spin  $S_{\text{tot}}$  is nonzero in the presence of a magnetic field, coupling of the moments to the singlet ( $A$ ) and triplet ( $T_2$ ) phonon modes can no longer be neglected. Still, when the applied magnetic field is weak, the distortion is such that the crystal retains a tetragonal symmetry. The spins develop a canted antiferromagnetic order with two frustrated bonds and four antiferromagnetic bonds. As the field strength increases, the doublet force  $|\mathbf{f}^E| = (4/\sqrt{3})(S^2 - S_{\text{tot}}^2/16)$  decreases as a result of the increasing total spin. At a critical field, the trigonal distortion, accompanying a 3-up-1-down collinear spin configuration maximizing the triplet forces,  $f_i^{T_2} = \sqrt{2}S^2$ ,

becomes more favorable energetically. The tetragonal distortion thus gives way to the trigonal one through a discontinuous transition.

Using the bond-phonon model, Penc and co-workers [30] obtained a classical phase diagram for the spin-Jahn-Teller effect in a single tetrahedron. The transition to the collinear 3:1 states takes place at a field strength  $H \approx 3J$  and  $J'^2/k \gtrsim 0.05J$ . A general symmetry analysis also showed that the collinear 3:1 states are always stabilized over a finite range of magnetic field, provided that  $J^{E'} < 2J^{T'_2}$  [30].

Similar to the ground-state manifold at zero field, the model with independent bonds retains an extensively degenerate manifold of half-magnetization states, because the trigonal distortion of individual tetrahedra can be along any of the four  $\langle 111 \rangle$  axes. This accidental degeneracy is lifted by the additional coupling term (1.15) introduced by the site-phonon model, which favors an antidistortive coupling between neighboring tetrahedra. Using this rule, Bergman *et al.* [27] showed that a unique spin configuration (up to discrete lattice symmetries) with a quadrupled, cubic unit cell is the ground state of the system in the half-magnetization plateau. The resulting space group,  $P4_332$ , is consistent with the X-ray diffraction pattern of the spinel  $\text{HgCr}_2\text{O}_4$  [31].

## 1.4 Collective Spin-Jahn-Teller effect on the pyrochlore lattice

Attempts to extend the analysis of the spin-Jahn-Teller effect on a single tetrahedron to an infinite pyrochlore lattice encounter a conceptual problem: there are *infinitely many* phonon modes coupled to the spins (one may expect two for every tetrahedron). There are also technical difficulties: detailed knowledge of the crystal's elastic properties is required. As a result of these difficulties, the problem lacks a general solution.

Some progress may, however, be made through the use of local phonon models, as described in the previous section. Still, a massive accidental degeneracy remains in the ground states of these simplified models. Further, the lattice modes in real crystals are plane waves, and thus a lattice distortion involves only a small number of phonons with specific lattice momenta. For example, the distortion in  $\text{ZnCr}_2\text{O}_4$  shows superlattice peaks in a diffraction experiment with wavenumbers  $[\frac{1}{2} \frac{1}{2} \frac{1}{2}]$  [10]. This does make it possible to take an alternative, phenomenological approach in which only a small number of lattice modes is considered. Such an approach was taken by Tchernyshyov *et al.* [15], who considered the simplest case where spin displacements preserve the translational symmetries of the lattice and break only point-group symmetries.

The pyrochlore lattice is made up of tetrahedra of two different orientations. Because all tetrahedra of the same orientation are related by lattice translation (which is assumed to remain a good symmetry), it is necessary

to consider only two tetrahedra of opposite orientations  $A$  and  $B$  (Fig. 1.5). The symmetry group must be expanded from  $T_d$  by including the inversion  $I$  exchanging the two sublattices of tetrahedra,  $T_d \otimes I = O_h$  [13]. The irreps remain largely unaltered, with the exception of a newly added parity index, which enters because these are either even ( $g$ ) or odd ( $u$ ) under the inversion.

At linear order in the displacements, the only modes which couple to the spins are the doublets  $E_g$  and  $E_u$ . The former represents an overall tetragonal or orthorhombic distortion of the lattice, while the latter is an optical phonon with wavenumber  $\mathbf{q} = 0$  that distorts tetrahedra of opposite orientations in exactly opposite ways (*e.g.* by flattening tetrahedra  $A$  and elongating tetrahedra  $B$  by the same amount and in the same direction). These modes can be expressed in terms of linear combinations of distortions on tetrahedra of types  $A$  and  $B$ ,

$$\mathbf{Q}^g = \frac{\mathbf{Q}^A + \mathbf{Q}^B}{\sqrt{2}}, \quad \mathbf{Q}^u = \frac{\mathbf{Q}^A - \mathbf{Q}^B}{\sqrt{2}}. \quad (1.16)$$

The spin-lattice energy (1.8) generalizes to

$$E(\mathbf{f}^A, \mathbf{f}^B, \mathbf{Q}^A, \mathbf{Q}^B) = J'(\mathbf{Q}^A \cdot \mathbf{f}^A + \mathbf{Q}^B \cdot \mathbf{f}^B) + k_g |\mathbf{Q}^g|^2/2 + k_u |\mathbf{Q}^u|^2/2, \quad (1.17)$$

where  $k_g$  and  $k_u$  are the elastic constants of the even and odd  $E$  doublets. Minimization with respect to the lattice modes  $\mathbf{Q}^g$  and  $\mathbf{Q}^u$  yields the energy as a function of the spin variables in the form

$$\begin{aligned} E(\mathbf{f}^A, \mathbf{f}^B) &= -\frac{K_g |\mathbf{f}^A + \mathbf{f}^B|^2}{4} - \frac{K_u |\mathbf{f}^A - \mathbf{f}^B|^2}{4} \\ &= -\frac{(K_g + K_u) (|\mathbf{f}^A|^2 + |\mathbf{f}^B|^2)}{4} \\ &\quad - \frac{(K_g - K_u) (\mathbf{f}^A \cdot \mathbf{f}^B)}{2}, \end{aligned} \quad (1.18)$$

where we have introduced the effective magnetoelastic exchange couplings  $K_{g,u} = J'^2/k_{g,u}$ .

The second line in Eq. (1.18) is the result familiar from Eq. (1.13): the magnitude of the doublet force  $\mathbf{f}$  is maximized on tetrahedra of both sublattices. Thus one expects to find states with collinear spins and (for  $J' < 0$ ) tetrahedra flattened along one of the three  $\langle 100 \rangle$  directions. The third line in Eq. (1.18) represents a coupling between the  $\mathbf{f}$  variables of the two sublattices, whose consequences depend on which of the two lattice modes is softer.

If  $K_g > K_u$  ( $E_g$  mode softer), the energy is minimized when  $\mathbf{f}^A$  and  $\mathbf{f}^B$  are in the same corner of the force triangle (Fig. 1.2). Tetrahedra of both sublattices are flattened along the same  $\langle 100 \rangle$  direction, so that only an  $E_g$  distortion is present. The spin configuration is shown in Fig. 1.4. The magnetic unit cell coincides with the structural one. Because we are considering an  $O(3)$ -symmetric Heisenberg model, the global orientation of the spins can be arbitrary

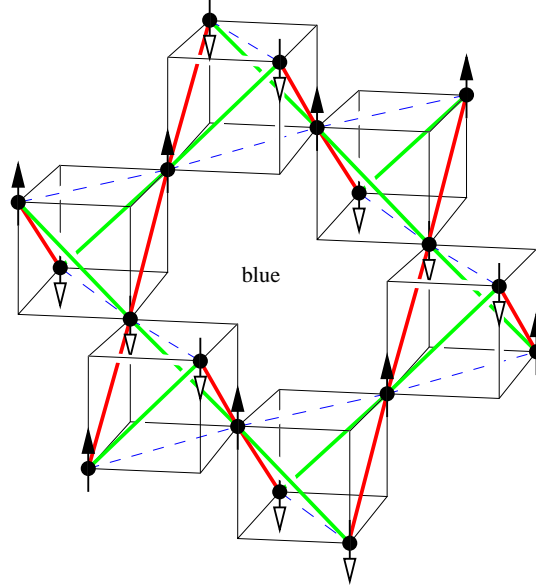


**Fig. 1.4.** Magnetic order in a state with a softer  $E_g$  mode. Frustrated bonds are shown as dashed lines. The lattice is flattened uniformly (for  $J' < 0$ ). Reprinted with permission from Ref. [15].

If, on the other hand,  $K_g < K_u$  (softer  $E_u$  mode), the two  $\mathbf{f}$  vectors are located in different corners of the triangle, so that tetrahedra of types  $A$  and  $B$  are flattened along two different  $\langle 100 \rangle$  directions, giving six possible ground states. The distortion is a superposition of the  $E_u$  and  $E_g$  modes. The presence of the even mode is understood in a straightforward manner: if tetrahedra of type  $A$  are flattened along  $\langle 100 \rangle$  and tetrahedra of type  $B$  along  $\langle 010 \rangle$ , the lattice is on average *elongated* along  $\langle 001 \rangle$ . The presence of the  $E_u$  component of the distortion means that the inversion symmetry is broken spontaneously. This has important consequences for the magnetic order, shown in Fig. 1.5, as we discuss in detail below. Here we note only that frustrated bonds form left-handed spirals in this particular state.

### 1.5 Collective Jahn-Teller effect in $\text{CdCr}_2\text{O}_4$

The normal spinels  $\text{ACr}_2\text{O}_4$  (where  $A$  is a nonmagnetic Zn, Mg, Cd, or Hg ion) are strongly frustrated antiferromagnets exhibiting the spin-induced Jahn-Teller distortion. The magnetic  $\text{Cr}^{3+}$  ions forming the pyrochlore lattice have electronic configuration  $3d^3$ . The oxygen octahedron surrounding the chromium ion splits the  $3d$  levels into a high-energy  $e_g$  doublet and a low-energy  $t_{2g}$  triplet; the former are unoccupied while the latter are singly

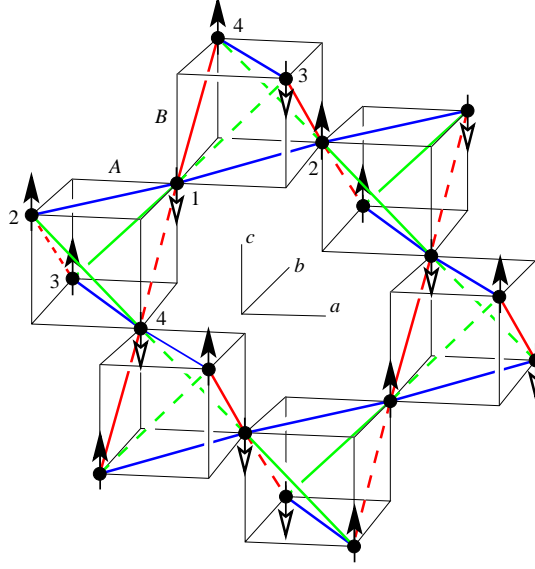


**Fig. 1.5.** Magnetic order in a state with a softer  $E_u$  mode. Frustrated bonds are shown as dashed lines. Tetrahedra of the two different orientations (labeled A and B) are flattened along axes  $a$  and  $b$ , so that the net distortion of the lattice is (for  $J' < 0$ ) an elongation along axis  $c$ . Reprinted with permission from Ref. [32].

occupied, with the 3 electrons having parallel spins. Thus the orbital degree of freedom is quenched and the spins form a nearly isotropic magnetic moment with total spin  $S = 3/2$  and a gyromagnetic ratio of  $g = 2$  [8]. Interactions between the spins are mediated mostly by direct antiferromagnetic exchange between neighboring Cr sites [18] (with the exception of  $\text{HgCr}_2\text{O}_4$ , where this contribution is comparable to the ferromagnetic superexchange term mediated by the oxygen ions).

All of these compounds have a strongly correlated paramagnetic state well below their Curie-Weiss temperatures,  $\Theta$ , and order magnetically at a temperature  $T_N \ll \Theta$ . The phase transition is discontinuous and is accompanied by a lattice distortion [8–10]. The lack of orbital degrees of freedom points to a magnetoelastic origin for the lattice distortion.

$\text{CdCr}_2\text{O}_4$  is the best-understood system to date. In the distorted state below  $T_N$  it shows no superlattice peaks [9], indicating that the translational symmetry of the high-temperature cubic phase (space group  $Fd\bar{3}m$ ) remains unchanged. The point-group symmetry is lowered: the lattice exhibits a tetragonal distortion with lattice constants  $a = b < c$  (an overall elongation). The low-temperature structure was identified by Chung *et al.* as the pyrochlore lattice with a uniform tetragonal elongation (space group  $I4_1/amd$ ) [9], *i.e.* a pure  $E_g$  distortion. However, as listed next, there are good reasons to believe

that this distortion also involves the staggered component  $E_u$ , which breaks the inversion symmetry and lowers the space group down to  $I4_122$ .

1. The dominance of direct antiferromagnetic exchange between adjacent chromium spins means that the exchange constant decreases with increasing ionic separation, *i.e.*  $J' < 0$ . If the distortion were of pure  $E_g$  type, the crystal would flatten along one axis, yielding  $a = b > c$  in contradiction to the experimental data [9]. As explained in the previous section, an  $E_u$ -driven distortion would lead to an overall elongation of the lattice,  $a = b < c$ , in agreement with the experiment.

2. An  $E_u$  distortion breaks the inversion symmetry of the crystal, making the crystalline lattice *chiral*. Indeed, the elongated (frustrated) bonds in Fig. 1.5 form spirals of one helicity. Spin-orbit coupling in the form of the Dzyaloshinskii-Moriya interaction would then spread the chirality from the lattice to the spins, generating a spiral magnetic order. The observed magnetic order in  $\text{CdCr}_2\text{O}_4$  is in fact a weakly incommensurate spiral [9].

### 1.5.1 Spiral magnetic order in $\text{CdCr}_2\text{O}_4$

Chung *et al.* reported an incommensurate magnetic order with magnetic Bragg peaks at  $\mathbf{q} = 2\pi(0, \delta, 1)$  in a crystal with an elongated  $c$  axis ( $a = b = 0.995c$ ) and  $\delta = 0.09$ . The magnetization lies in the  $ac$ -plane. Because the incommensurability  $\delta$  is small, the magnetic order can be understood as a commensurate state with  $\mathbf{q} = 2\pi(0, 0, 1)$  twisting slowly along the  $b$ -direction.

The same authors found two such structures which would be consistent with the data they obtained from elastic neutron scattering. One of the proposed ordering patterns is derived from the commensurate state shown in Fig. 1.5, and is precisely what one expects when the magnetoelastic effect is driven by the  $E_u$  phonon. The other candidate is derived from an “orthogonal” state where the spins on every tetrahedron are oriented, for example, in directions  $+\hat{\mathbf{x}}$ ,  $-\hat{\mathbf{x}}$ ,  $+\hat{\mathbf{y}}$ , and  $-\hat{\mathbf{y}}$ . Such a state is very hard to obtain through the spin-driven Jahn-Teller effect [15], and no other justification for this state is currently known.

The small value of  $\delta$  makes it possible to treat this incommensurability as the result of a weak perturbation on top of the Heisenberg exchange and magnetoelastic coupling. Chern *et al.* [32] derived possible magnetic spiral states that arise when the Dzyaloshinskii-Moriya interaction is added to these two energy terms. These authors found two candidate solutions, one of which is entirely consistent with the data of Chung *et al.* This analysis and its results are described in the next section.

### 1.5.2 Theory of spiral magnetic order

The Dzyaloshinskii-Moriya (DM) interaction gives a contribution

$$H_{\text{DM}} = \sum_{\langle ij \rangle} \mathbf{D}_{ij} \cdot [\mathbf{S}_i \times \mathbf{S}_j], \quad (1.19)$$



to the Hamiltonian, where the sum extends over pairs of nearest neighbors. This term is allowed on the ideal pyrochlore lattice, where the bonds are not centrosymmetric, the precondition for a non-vanishing coupling constant  $\mathbf{D}_{ij}$ . At the same time, the high symmetry of the lattice constrains the direction of this vector [33]: for a bond oriented along the  $[110]$  lattice direction, the vector must point along  $[1\bar{1}0]$  ( $\mathbf{D}_{ij} = (\pm D, \mp D, 0)/\sqrt{2}$ ). The value of  $\mathbf{D}_{ij}$  on any other bond is then found through the symmetry transformations of the system. In a collinear magnetic state, the expectation value of  $H_{\text{DM}}$  is zero, but its contribution can be lowered by twisting the spins into a spiral.

The pitch of the spiral is determined by the competition between the DM coupling strength  $D$  and a spin stiffness. In most antiferromagnets, the spin stiffness is set by the exchange interaction, but the pyrochlore antiferromagnet with nearest-neighbor exchange is an exception: the large degeneracy of its ground state leads to a vanishing stiffness. As a result, the ground state in the presence of the DM interaction is not a long-range spiral but is rather a commensurate state with noncollinear spins [33].

The presence of magnetoelastic interactions changes the situation. Recall that the spin-induced Jahn-Teller effect selects a state with collinear spins. This tendency towards collinear states results in a finite spin stiffness. As a result, the pitch of the spiral is a quantity of order  $D/K$ , where  $K = J'^2/k$  is the effective magnetoelastic interaction.

A problem where the nearest-neighbor exchange  $J$ , the magnetoelastic energy scale  $K$ , and the DM coupling  $D$  are each arbitrary is hard to solve analytically. However, it simplifies if these energy scales are well separated, the conventional hierarchy being

$$JS^2 \gg KS^4 \gg DS^2. \quad (1.20)$$

A quantitative analysis indicates that in  $\text{CdCr}_2\text{O}_4$  these scales are of similar magnitude (as discussed at the end of this section), but still have the expected order,  $JS^2 > KS^4 > DS^2$ . Thus while a theory based on the assumption (1.20) may not provide a quantitative account of magnetic order in  $\text{CdCr}_2\text{O}_4$ , it presents at minimum a good point of departure for understanding it.

Minimization of the dominant term, the exchange energy (1.1), yields a constraint that the total spin be zero on every tetrahedron. The remaining degrees of freedom of a single tetrahedron can be parametrized using the staggered magnetizations

$$\mathbf{L}_1 = \frac{\mathbf{S}_1 - \mathbf{S}_2 - \mathbf{S}_3 + \mathbf{S}_4}{4S}, \mathbf{L}_2 = \frac{-\mathbf{S}_1 + \mathbf{S}_2 - \mathbf{S}_3 + \mathbf{S}_4}{4S}, \mathbf{L}_3 = \frac{-\mathbf{S}_1 - \mathbf{S}_2 + \mathbf{S}_3 + \mathbf{S}_4}{4S}.$$

Because each spin belongs to two tetrahedra, the staggered magnetizations on one sublattice of tetrahedra determine completely those of the other sublattice. We use the staggered magnetizations of sublattice  $A$ ,  $\{\mathbf{L}_i^A\}$ , to express the magnetizations of sublattice  $B$ , and, except in cases of possible confusion, suppress the sublattice index to simplify the notation.

Even for a single tetrahedron, the three staggered magnetizations are not completely independent. Vanishing of the total spin in the ground state makes them mutually orthogonal and imposes on their lengths the constraint [34]

$$\mathbf{L}_i = L_i \hat{\mathbf{l}}_i, \quad \hat{\mathbf{l}}_i \cdot \hat{\mathbf{l}}_j = \delta_{ij}, \quad \sum_{i=1}^3 L_i^2 = 1. \quad (1.21)$$

The lengths  $L_i$  parametrize the angles between the spins and are related to the bond doublet  $\mathbf{f}$  by

$$f_1 = 2S^2 (L_1^2 + L_2^2 - 2L_3^2)/\sqrt{3}, \quad f_2 = 2S^2 (L_1^2 - L_2^2). \quad (1.22)$$

Thus five parameters are required to describe the magnetic state of a tetrahedron in the ground state of Eq. (1.1): three Euler angles for the triad  $\{\hat{\mathbf{l}}_i\}$  and two further parameters for the bond doublet, *e.g.*  $\mathbf{f} = (f_1, f_2)$ .

The magnetic order of  $\text{CdCr}_2\text{O}_4$  in the commensurate limit  $\delta \rightarrow 0$  (Fig. 1.5) has staggered site magnetizations:  $\mathbf{L}_2 = \mathbf{L}_3 = 0$  and  $\mathbf{L}_1 = e^{i\mathbf{q}\cdot\mathbf{r}} \hat{\mathbf{n}}_1$ , where  $\mathbf{q} = 2\pi(0, 0, 1)$  and  $\hat{\mathbf{n}}_1$  is an arbitrary unit vector. In terms of the three staggered magnetizations, the DM term for a single tetrahedron is

$$E_{\text{DM}} = -DS^2 (\hat{\mathbf{a}} \cdot \mathbf{L}_2 \times \mathbf{L}_3 + \hat{\mathbf{b}} \cdot \mathbf{L}_3 \times \mathbf{L}_1 + \hat{\mathbf{c}} \cdot \mathbf{L}_1 \times \mathbf{L}_2). \quad (1.23)$$

It is easy to see that the DM energy is exactly zero for the collinear state. For either sign of  $D$ , this term can be made negative by allowing a small component of  $\mathbf{L}_2$  or  $\mathbf{L}_3$ , which describes a twisting spin configuration. The lowering of the DM energy (1.23) is accompanied by an increase of the magnetoelastic energy. However, further analysis shows that the former is linear in  $\mathbf{L}_2$  and  $\mathbf{L}_3$  while the latter is quadratic, so that such a twisting distortion always occurs.

To pass to a continuum description, we express the rapidly oscillating unit vectors  $\hat{\mathbf{l}}_i = \hat{\mathbf{n}}_i e^{i\mathbf{q}\cdot\mathbf{r}}$  in terms of a slowly varying orthonormal triad  $\{\hat{\mathbf{n}}_i\}$ , and use the length constraint (1.21) to eliminate  $L_1$  by

$$\mathbf{L}_1 = \left(1 - \frac{L_2^2 + L_3^2}{2}\right) \hat{\mathbf{n}}_1 e^{i\mathbf{q}\cdot\mathbf{r}}, \quad \mathbf{L}_2 = L_2 \hat{\mathbf{n}}_2 e^{i\mathbf{q}\cdot\mathbf{r}}, \quad \mathbf{L}_3 = L_3 \hat{\mathbf{n}}_3 e^{i\mathbf{q}\cdot\mathbf{r}}. \quad (1.24)$$

At this point, the magnetic structure is described in terms of five slowly varying fields,  $L_2$ ,  $L_3$ , and the triad  $\{\hat{\mathbf{n}}_i\}$ .

The number of independent fields can be further reduced by examining tetrahedra of sublattice  $B$ : the vector of total magnetization on each  $B$  tetrahedron must vanish, giving three more constraints. The total spin of a  $B$  tetrahedron centered at  $\mathbf{r}^B = \mathbf{r}^A + (1/4, 1/4, 1/4)$  is given by

$$\mathbf{M}^B(\mathbf{r}^B) = \mathbf{S}_1(\mathbf{r}^A + \mathbf{a}_1) + \mathbf{S}_2(\mathbf{r}^A + \mathbf{a}_2) + \mathbf{S}_3(\mathbf{r}^A + \mathbf{a}_3) + \mathbf{S}_4(\mathbf{r}^A),$$

where  $\mathbf{a}_1 = (0, 1/2, 1/2)$ ,  $\mathbf{a}_2 = (1/2, 0, 1/2)$ , and  $\mathbf{a}_3 = (1/2, 1/2, 0)$  are primitive lattice vectors (the centers of the tetrahedra form a diamond lattice; the Bravais lattice is fcc). Expressing the spins  $\{\mathbf{S}_i\}$  in terms of the staggered

magnetizations  $\{\mathbf{L}_i\}$  and using the gradient expansion, one obtains, to the lowest orders in  $L_2$ ,  $L_3$ , and the gradients, the constraint

$$\mathbf{M}^B = L_3 \hat{\mathbf{n}}_3 - \frac{1}{4} \frac{\partial \hat{\mathbf{n}}_1}{\partial y} = 0. \quad (1.25)$$

Thus it is clear that  $L_3$  and  $\hat{\mathbf{n}}_3$  are determined by the gradient  $\nabla \hat{\mathbf{n}}_1$ .

In a similar way, expressing the staggered magnetizations on sublattice  $B$  to lowest order in  $\nabla \hat{\mathbf{n}}_1$  leads to

$$\mathbf{L}_1^B = L_2 \hat{\mathbf{n}}_2 - \frac{1}{4} \frac{\partial \hat{\mathbf{n}}_1}{\partial z}, \quad \mathbf{L}_2^B = \hat{\mathbf{n}}_1, \quad \mathbf{L}_3^B = -\frac{1}{4} \frac{\partial \hat{\mathbf{n}}_1}{\partial x}. \quad (1.26)$$

Substituting these expressions into Eq. (1.23) and adding contributions from tetrahedra of both types yields

$$E_{\text{DM}} = -\frac{1}{4} DS^2 \hat{\mathbf{n}}_1 \cdot \left( \hat{\mathbf{a}} \times \frac{\partial \hat{\mathbf{n}}_1}{\partial x} + \hat{\mathbf{b}} \times \frac{\partial \hat{\mathbf{n}}_1}{\partial y} - \hat{\mathbf{c}} \times \frac{\partial \hat{\mathbf{n}}_1}{\partial z} \right). \quad (1.27)$$

The DM energy contains terms linear in gradients of  $\hat{\mathbf{n}}_1$ , indicating that the spins are unstable against the formation of spiral configurations. As an example, the first term  $\hat{\mathbf{n}}_1 \cdot \hat{\mathbf{a}} \times \partial \hat{\mathbf{n}}_1 / \partial x$  favors a magnetic order with the unit vector  $\hat{\mathbf{n}}_1$  perpendicular to the  $a$ -axis and spiraling about it.

As discussed previously, the spin stiffness has its origin in the magnetoelastic energy. For simplicity, here we consider only distortions due to  $E_u$  phonons and neglect the effect of  $E_g$  distortions (a procedure definitely appropriate in the limit  $K_g \ll K_u$ ). The linear decrease of the DM energy due to gradients of  $\hat{\mathbf{n}}_1$  must be balanced by the increase in magnetoelastic energy, which on symmetry grounds must be quadratic in  $\nabla \hat{\mathbf{n}}_1$ . From Eq. (1.18), the increase of magnetoelastic energy is  $E_{\text{me}} = -K_u \mathbf{u}_0 \cdot \delta \mathbf{u} / 2$ , where  $K_u = J^2 / k_u$  and  $\mathbf{u} = \mathbf{f}^A - \mathbf{f}^B$ . The unperturbed odd doublet is  $\mathbf{u}_0 = 4S^2 (0, 1)$ . Because we are describing the spiral magnetic order in terms of the staggered magnetizations, it is convenient to use Eq. (1.22) for the calculation of  $\delta \mathbf{f}^A$  and  $\delta \mathbf{f}^B$ . Retaining terms to second order in  $\nabla \hat{\mathbf{n}}_1$  leads to

$$E_{\text{me}} = \frac{K_u S^4}{4} \left[ \left( \frac{\partial \hat{\mathbf{n}}_1}{\partial x} \right)^2 + \left( \frac{\partial \hat{\mathbf{n}}_1}{\partial y} \right)^2 + 2 \left( \frac{\partial \hat{\mathbf{n}}_1}{\partial z} \right)^2 - L_2 \hat{\mathbf{n}}_2 \cdot \frac{\partial \hat{\mathbf{n}}_1}{\partial z} + 4L_2^2 \right]. \quad (1.28)$$

Because the DM energy (1.27) does not depend on  $L_2$ , minimization of the total energy with respect to  $L_2$  affects only the magnetoelastic term (1.28) and yields

$$L_2 = \frac{1}{8} \hat{\mathbf{n}}_2 \cdot \frac{\partial \hat{\mathbf{n}}_1}{\partial z}; \quad (1.29)$$

thus  $L_2$  is also eliminated. The minimized magnetoelastic energy is

$$E_{\text{me}} = \frac{K_u S^4}{4} \left[ \left( \frac{\partial \hat{\mathbf{n}}_1}{\partial x} \right)^2 + \left( \frac{\partial \hat{\mathbf{n}}_1}{\partial y} \right)^2 + 2 \left( \frac{\partial \hat{\mathbf{n}}_1}{\partial z} \right)^2 - \left( \hat{\mathbf{n}}_2 \cdot \frac{\partial \hat{\mathbf{n}}_1}{\partial z} \right)^2 \right]. \quad (1.30)$$

The total energy of the spiral state, now expressed as a functional of the vector fields  $\hat{\mathbf{n}}_1(\mathbf{r})$  and  $\hat{\mathbf{n}}_2(\mathbf{r})$ , is the sum of Eqs. (1.27) and (1.30). Its minimization yields a second-order partial differential equation. While we are unable to find the most general solution to this equation, we can find three highly symmetrical spiral solutions in which the spins remain perpendicular to, while twisting about, one of the  $\langle 100 \rangle$  axes. As one example, a spiral state along the  $b$  axis is described by  $\hat{\mathbf{n}}_1 = (\cos \theta(y), 0, \sin \theta(y))$  and has total energy

$$E = -(DS^2\theta' + K_u S^4\theta'^2)/4, \quad (1.31)$$

where  $\theta' = d\theta/dy$ . Minimization of this quantity gives the pitch of the spiral,

$$\theta' = 2\pi\delta = \frac{D}{2K_u S^2}. \quad (1.32)$$

Equation (1.29) implies that  $\mathbf{L}_2^A = 0$ ; the  $A$  tetrahedra therefore have coplanar spins spanned by two orthogonal Néel vectors,  $\mathbf{L}_1^A$  and  $\mathbf{L}_3^A$ . The angles between spin pairs are given by  $\theta_{14} = \theta_{23} = 2L_3$ . From Eq. (1.25), this angle is related to the pitch by  $2L_3 = \pi\delta$ . The spiral magnetic state has the structure

$$\begin{aligned} \mathbf{L}_1^A &= \cos(\pi\delta/2) (\cos(2\pi\delta y), 0, \sin(2\pi\delta y)) e^{2\pi iz}, \\ \mathbf{L}_2^A &= 0, \\ \mathbf{L}_3^A &= \sin(\pi\delta/2) (-\sin(2\pi\delta y), 0, \cos(2\pi\delta y)) e^{2\pi iz}, \end{aligned} \quad (1.33)$$

producing Bragg scattering at wavevector  $\mathbf{q} = 2\pi(0, \pm\delta, 1)$ , while the ordered magnetic moments lie in the  $ac$ -plane [Fig. 1.6(b)]. All of this is consistent with the experimental data of Ref. [9].

It is worth noting that the distorted crystal structure preserves certain symmetries on interchanging the  $A$  and  $B$  sublattices, such as inversion at a Cr site followed by a  $\pi/2$  rotation in the  $ab$ -plane. However, the magnetic order described here breaks these symmetries. From Eq. (1.26) one has  $\mathbf{L}_1^B = \mathbf{L}_3^B = 0$ , which means that every tetrahedron on sublattice  $B$  has collinear spins, whereas the spins of the  $A$  tetrahedra are twisted into a (weakly) non-collinear state. This disparity between the two sublattices should result in different distortions of the two types of tetrahedra, thus further lowering the symmetry of the crystal. However, the magnitude of the additional distortion is expected to be small because the degree of non-collinearity is small,  $\delta \ll 1$ .

Spiral states in which the spins rotate about the  $a$ -axis [Fig. 1.6(a)] can be obtained similarly, by using the ansatz  $\hat{\mathbf{n}}_1 = (0, \cos \theta(x), \sin \theta(x))$ . The resulting solution can also be obtained from Eq. (1.33) through symmetry operations which exchange the two sublattices of tetrahedra, such as inversion on a Cr site. This spiral produces a magnetic Bragg peak at  $\mathbf{q} = (\mp\delta, 0, 1)$ .

Finally, there is a third spiral solution, shown in Fig. 1.6(c), where the spins twist about the  $c$ -axis. In this state, which is not related to the other two solutions by any symmetry, the magnetic Bragg peak occurs at  $\mathbf{q} = 2\pi(0, 0, 1 + \delta)$  and both sublattices have tetrahedra with coplanar, rather than

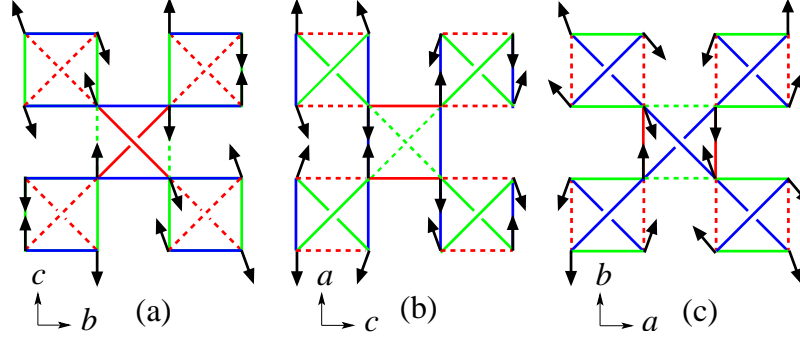


**Fig. 1.6.** Three symmetrical spiral magnetic structures minimizing the energy. The spins are perpendicular to and twist about the *a*-axis (a), *b*-axis (b), or *c*-axis (c). Dashed lines indicate frustrated bonds. The crystal is viewed along a  $\langle 100 \rangle$  direction. Reprinted with permission from Ref. [32].

collinear, spins. That this spiral state has the same energy as the previous two is a coincidence: its total energy is also given by Eq. (1.31) with  $\theta' = d\theta/dz$ . This degeneracy is lifted when other perturbations, such as further-neighbor interactions, are taken into account.  $\text{CdCr}_2\text{O}_4$  has a significant *third*-neighbor antiferromagnetic exchange interaction, which acts to favor strongly the states with spirals twisting along the *a*- or *b*-axis [32].

In closing this section, we comment on the assumption (1.20) of well-separated energy scales in the problem. *Ab initio* calculations [32] yield a nearest-neighbor exchange energy  $JS^2 = 1.1$  meV and a magnetoelastic energy  $K_u S^4 = 0.76$  meV. The strength of the DM interaction can be estimated from the measured pitch of the spiral,  $\delta = 0.09$ , using Eq. (1.32), which gives  $DS^2 = 0.21$  meV. While the three energy scales are not vastly different, they do appear in the correct order of decreasing magnitude,  $JS^2 > K_u S^4 > DS^2$ .

## 1.6 Summary and open questions

The spinel compound  $\text{CdCr}_2\text{O}_4$  provides an opportunity to test our understanding of the ground state of the Heisenberg antiferromagnet on the pyrochlore lattice. When the lattice degrees of freedom are included, both the selected magnetic order and the lattice distortion are in agreement with a theoretical model [15] based on two vibrational doublets of the crystal, the  $\mathbf{q} = 0$  optical phonon  $E_u$  and the uniform lattice distortion  $E_g$ . The model ties the incommensurate nature of the spiral magnetic order to a spontaneous breaking of the inversion symmetry in the crystal, which has not yet been observed directly in  $\text{CdCr}_2\text{O}_4$ .

The magnetoelastic phase transition between the high-*T* correlated paramagnet [35] and the low-*T* ordered phase remains poorly understood. It is

strongly discontinuous in both  $\text{ZnCr}_2\text{O}_4$  [8] and  $\text{CdCr}_2\text{O}_4$  [9], with both the lattice distortion and the ordered moment reaching their  $T = 0$  values immediately below the ordering temperature. A Landau free-energy approach based on the spin-Peierls order parameter (1.7) appears to be the only candidate approach available for modeling the underlying physics [15]. However, it is not evident that this phenomenology can provide a full description. In  $\text{CdCr}_2\text{O}_4$ , the order parameter has the  $E_u$  symmetry and does not allow for a cubic invariant in the free energy, thus excluding the most obvious cause for a discontinuous phase transition. The phase transition may yet turn out to be first-order if the even ( $E_g$ -symmetric) order parameter is nearly soft [15], but this question has not yet been clarified. In fact it remains unclear whether the valence-bond variables (1.7) represent a good choice of the order parameter for these systems: the low- $T$  phase in both  $\text{ZnCr}_2\text{O}_4$  and  $\text{CdCr}_2\text{O}_4$  is magnetically ordered, suggesting that a type of staggered magnetization may be a more appropriate choice.

Finally, a realistic model of this phase transition must take into account the entropy of the correlated paramagnetic state [4]. The very high entropy of the disordered phase may be responsible for the discontinuous nature of the phase transition, as has been demonstrated for the case of lattice models with large numbers of flavors [36].

## References

1. A.P. Ramirez, J. Appl. Phys. **70**, 5952 (1991)
2. D.A. Huse, A.D. Rutenberg, Phys. Rev. B **45**, 7536 (1992)
3. M.J. Harris, M.P. Zinkin, Z. Tun, B.M. Wanklyn, I.P. Swainson, Phys. Rev. Lett. **73**, 189 (1994)
4. R. Moessner, J.T. Chalker, Phys. Rev. B **58**, 12049 (1998)
5. J.T. Chalker, P.C.W. Holdsworth, E.F. Shender, Phys. Rev. Lett. **68**, 855 (1992)
6. C. Kittel, Phys. Rev. **120**, 335 (1960)
7. I.S. Jacobs, J.W. Bray, H.R. Hart, L.V. Interrante, J.S. Kasper, G.D. Watkins, D.E. Prober, J.C. Bonner, Phys. Rev. B **14**, 3036 (1976)
8. S.H. Lee, C. Broholm, T.H. Kim, W. Ratcliff, S.W. Cheong, Phys. Rev. Lett. **84**, 3718 (2000)
9. J.H. Chung, M. Matsuda, S.H. Lee, K. Kakurai, H. Ueda, T.J. Sato, H. Takagi, K.P. Hong, S. Park, Phys. Rev. Lett. **95**, 247204 (2005)
10. H. Ueda, H. Mitamura, T. Goto, Y. Ueda, Phys. Rev. B **73**, 094415 (2006)
11. I. Bersuker, *The Jahn-Teller effect* (Cambridge University Press, Cambridge, 2006)
12. H.A. Jahn, E. Teller, Proc. Roy. Soc. London Ser. A **161**, 220 (1937)
13. L.D. Landau, E.M. Lifshitz, *Quantum mechanics: non-relativistic theory* (Butterworth-Heinemann, 1981)
14. Y. Yamashita, K. Ueda, Phys. Rev. Lett. **85**, 4960 (2000)
15. O. Tchernyshyov, R. Moessner, S.L. Sondhi, Phys. Rev. B **66**, 064403 (2002)
16. A.B. Harris, A.J. Berlinsky, C. Bruder, J. Appl. Phys. **69**, 5200 (1991)
17. K. Motida, S. Miyahara, J. Phys. Soc. Jpn. **28**, 1188 (1970)

18. A.B. Sushkov, O. Tchernyshyov, W. Ratcliff II, S.W. Cheong, H.D. Drew, Phys. Rev. Lett. **94**, 137202 (2005)
19. R.V. Aguilar, A.B. Sushkov, Y.J. Choi, S.W. Cheong, H.D. Drew, Phys. Rev. B **77**, 092412 (2008). DOI 10.1103/PhysRevB.77.092412
20. A. Olariu, P. Mendels, F. Bert, B.G. Ueland, P. Schiffer, R.F. Berger, R.J. Cava, Phys. Rev. Lett. **97**(16), 167203 (2006)
21. Y. Okamoto, M. Nohara, H. Aruga-Katori, H. Takagi, Phys. Rev. Lett. **99**(13), 137207 (2007)
22. F. Wang, A. Vishwanath, Phys. Rev. Lett. **100**, 077201 (2008)
23. T. Rudolf, C. Kant, F. Mayr, A. Loidl, Phys. Rev. B **77**, 024421 (2008). DOI 10.1103/PhysRevB.77.024421
24. F. Becca, F. Mila, Phys. Rev. Lett. **89**, 037204 (2002)
25. C. Weber, F. Becca, F. Mila, Phys. Rev. B **72**, 024449 (2005)
26. C. Jia, J.H. Nam, J.S. Kim, J.H. Han, Phys. Rev. B **71**, 212406 (2005)
27. D.L. Bergman, R. Shindou, G.A. Fiete, L. Balents, Phys. Rev. B **74**, 134409 (2006)
28. H. Ueda, H. Katori, H. Mitamura, T. Goto, H. Takagi, Phys. Rev. Lett. **94**, 047202 (2005)
29. H. Ueda, H. Mitamura, T. Goto, Y. Ueda, Phys. Rev. B **73**, 094415 (2006)
30. K. Penc, N. Shannon, H. Shiba, Phys. Rev. Lett. **93**, 197203 (2004)
31. M. Matsuda, H. Ueda, A. Kikkawa, Y. Tanaka, K. Katsumata, Y. Narumi, T. Inami, Y. Ueda, S.H. Lee, Nature Physics **3**, 397 (2007)
32. G.W. Chern, C.J. Fennie, O. Tchernyshyov, Phys. Rev. B **74**, 060405 (2006)
33. M. Elhajal, B. Canals, R. Sunyer, C. Lacroix, Phys. Rev. B **71**, 094420 (2005)
34. C.L. Henley, J. Appl. Phys. **61**, 3962 (1987)
35. S.H. Lee, C. Broholm, W. Ratcliff, G. Gasparovic, Q. Huang, T.H. Kim, S.W. Cheong, Nature **418**, 856 (2002)
36. S.B. Shlosman, R. Kotecký, Comm. Math. Phys. **83**, 493 (1981)